6

Temporal and Spatial Resolution Limit Study of Radiation Imaging Systems: Notions and Elements of Super Resolution

Faycal Kharfi, Omar Denden and Abdelkader Ali
Neutron Radiography Department/Nuclear Research Centre of Birine, Algeria

1. Introduction

The characterization of a radiographic imaging system response in terms of spatial and temporal resolution is a very important task that allows the determination of this system limits and capability in the investigation and visualization of very fast processes and of very small spatial details. Thus, the spatial and temporal resolutions limits are very important parameters of an imaging system that should be taken into consideration before the examination of any static object or dynamic process. The objectives of this chapter are the study and determination of radiation imaging system response in terms of spatial and temporal resolution limits and the application of super-resolution (SR) methods and algorithms to improve the resolution of captured neutron images or video sequences. The imaging system taken as example and being studied is a high-sensitivity neutron imaging system composed of an LiF+ZnS scintillator screen (0.25 mm thick), an Aluminium-coated mirror and a Charged Coupled Device (CCD) camera ($2x10^{-5}$ lx at F1.4).

The proposed approach and procedure for spatial resolution and system response determination is based on the establishment of the Modulation Transfer Function (MTF) using standard slanted edge method with the most appropriate algorithm selected according to previous studies. Temporal resolution study and characterization is a more complicated task that requires well understanding of video sequence capture process. In this chapter the limit of temporal resolution allowing minimum motion blur is studied according to a selected dynamic process capture and examination under different exposure conditions. Due to physical constraints (low L/D collimation ratio and weakness of neutron beam) and instrumental limitations of the used imaging system, the captured images or neutron video can be of low resolution. To overcome this limitation, super resolution methods and algorithms are applied to improve space-time resolution. The most used methods are: the iterative variation regularization methods, the methods based on information combing from low resolution frames, the methods of motion compensation and the SR filters.

All the mentioned procedures and approaches above are still available for any similar X-ray or Gamma imaging systems based on the same examination principle of radiation transmission. These methods and procedures are used to judge the ability of such imaging

system to produce spatial (internal details) and temporal (dynamic) properties of any moving object or dynamic process under examination.

This chapter is divided into three main parts. In the first one, the MTF determination is presented by proposing an accurate edge identification method and a line spread function under-sampling problem-resolving procedure. The proposed method and procedure were integrated into a MatLab code. The source code can be requested to the author of this chapter. In the second section, induced motion blur when a moving object is examined is studied as a function of video capture frame rate. This approach allows us to determine suitable exposure conditions and therefore the temporal resolution that enables an optimum image quality with minimum motion blur and noise and acceptable contrast. Finally, notions and elements of super resolution are presented in the last section with some interesting examples. The examples of resolution enhancement presented in this chapter concern a water flow process examined with the described neutron imaging system. Experimental results on real data sets confirm the electiveness of the proposed procedures and methodologies. All experiments were performed at the neutron radiography facility and laboratory of the Algerian Es-Salam research reactor.

2. Temporal and spatial resolution limit study of a radiographic imaging system

2.1 Spatial resolution limit determination

Spatial resolution limit is a very important parameter of an imaging system that should be taken into consideration before the examination of any object. In this first chapter part, we propose the determination of a neutron imaging system's response in terms of spatial resolution. The proposed procedure is based on establishment of the Modulation Transfer Function (MTF). The imaging system being studied is based on a high sensitivity CCD neutron camera ($2x10^{-5}$ lx at f1.4). The neutron beam used is issued from the horizontal beam port (H.6) of the Algerian Es-Salam research reactor. Our contribution in this field is in the MTF determination by proposing an accurate edge identification method and a line spread function undersampling problem-resolving procedure. These methods and procedure are integrated into a MatLab program (code). The methods, procedures and approaches proposed in this work are available for any other neutron imaging system and allow the judgment of the ability of a neutron imaging system to produce spatial properties of any object under examination.

The Modulation Transfer Function is a common metric used to quantify the spatial resolution in the system response. Traditional methods for MTF measurements were initially designed for devices forming consecutive images that can give erroneous MTF results, due to the fact that the sampling of digital devices is not properly taken into consideration. The slanted edge method, which is analogous to the impulse response determination for an electronic system, is a common technique used for the measurement of an accurate MTF because it requests a relatively simple experimental arrangement. In neutron imaging, this technique consists of imaging a thin and sharp slanted-edge onto the detector. The edge target must be made from a strong neutron absorbing material such as Gadolinium. The ISO 12233 standard presents the general methodology for MTF measurement based on this technique (Jespers et al., 1976). An interesting algorithms comparison work used for MTF measurement based on slanted-edge technique is presented in reference (Samei, et al., 2005).

The first goal of this chapter is to apply this methodology and to overcome some under-sampling and slanted edge identification difficulties, to establish an accurate MTF curve to be used for the determination of the system response and the effective spatial resolution limit of the neutron imaging system being studied (Domanus, 1992). The components of this imaging system are placed in an aluminium light tight box (175 mm x 105 mm x 120 mm) positioned vertically by a holder fixed on the metallic table of the neutron radiography facility. The camera consists of a 250 µm thick LiF–ZnS scintillator, a front-surfaced Al/SiO_2 mirror and a high sensitivity Sony CCD camera with $2x10^{-5}$ lx (at f1.4) as the minimum required illumination (Figure 1). It has a bit depth of 8 bits. The camera was manufactured and assembled by "Neutron Optics", France (www.NeutronOptics.com). According to the manufacturer specifications, this system has a maximum intrinsic spatial resolution of 200 µm (171.5 µm calculated). All necessary experiments were performed at the neutron radiography facility of the Es-Salam research reactor (Kharfi, et al., 2005). To achieve this task, a MatLab code was developed.

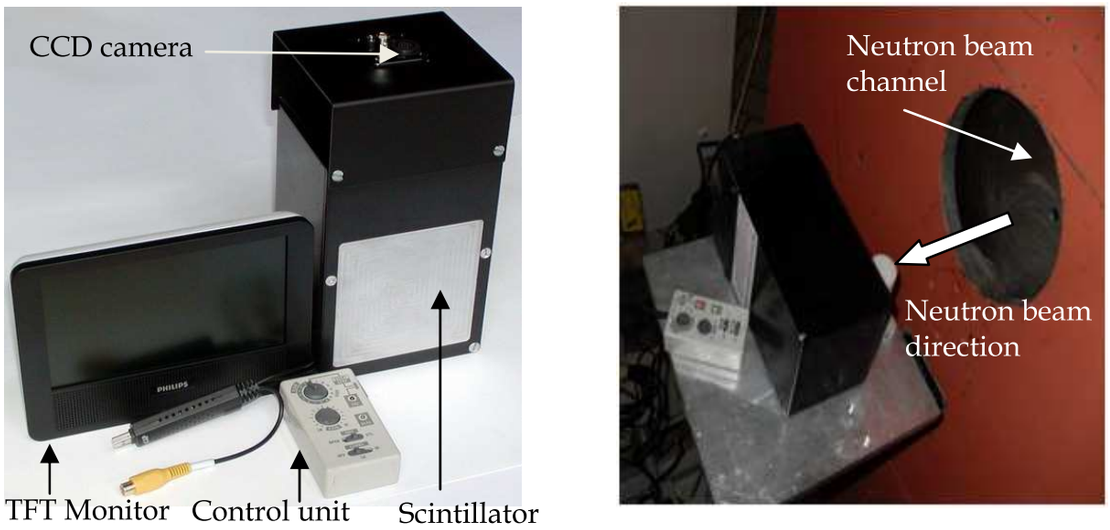

Fig. 1. The neutron imaging system studied.

2.1.1 Theoretical approach and experimental procedures

An MTF is the spatial frequency response of an imaging system. It characterizes the image sharpness produced by such systems. There are many methods allowing the determination of this function. One of them, based on analysis of a slanted-edge image of a suitable target, is used in this work. The methodology followed is described by the ISO 12233 standard. The advantages of this method are the simplicity and the minimal arrangement required during the experimental phase. The MTF curve is calculated from the Line Spread Function (LSF). LSF is computed by taking the first derivative of the Edge Spread Function (ESF). The ESF represent the pixel response in terms of gray levels along a line(s) perpendicular to the edge. Fourier transformation and subsequent normalization procedures are then applied to the LSF to compute the MTF (Estribau & Magnau, 2004). The MTF describes the amplitude or relevant contrast by which sine functions of different frequencies are moderated by an imaging system. It gives a measurement of the degradation when transferring data of the "physical" object to becoming an image. An MTF value of 1 indicates that the full amplitude

is transferred by the imaging system, while a MTF value of 0 indicates that no signal at all is transferred. In neutron imaging, an object can be represented in spatial domain by a 3D distribution function of neutron attenuation coefficients, a distribution of materials densities or any suitable distribution, and in the frequency domain by a distribution of frequencies that represent fine (high frequency) and coarse (low frequency) details. A good MTF must be sensitive to any change in the system input frequencies of the target or the examined object. For our case, the MTF deviation from the ideal value of 1 is due to: 1) the scintillator/mirror/CCD detector combination, 2) the geometrical exposure conditions, especially the beam divergent angle and the collimation ratio (L/D), and 3) the scattered neutrons. Indeed, a thorough understanding of exposure geometry and conditions, object or target input frequencies transferring and system response theory are very important for the establishment and correct analysis of the MTF obtained.

The slanted-edge method consists of imaging an edge onto the detector, slightly tilted with regard to the rows (or the columns) (Reichenbach et al., 1991). A slanted oriented edge, therefore, allows the horizontal Spatial Frequency Response (SFR) of the system to be obtained. In this case, the response of each pixel line across the edge gives a different ESF, due to the phasing of the pixel centre locations as the edge location changes with each row of pixels. These ESF are under-sampled but it is possible to mathematically increase the sampling rate by projecting data along the edge.

The main steps of the procedure used in this chapter to establish the MTF are the following:

1. Neutron radiography of the target, scanning of all lines and gray levels averaging and adjusting according to open beam and dark current images. This produces the ESF, also called the edge profile function. The distances in pixels are corrected depending on the angle of the edge slope. The edge should be sloped for smooth averaging.
2. Taking the first derivative from the ESF to generate the LSF.
3. Applying a discrete Fourier transform to the LSF. This produces the MTF.

In this chapter, a MATLAB code based on the Slanted-edge method was developed. This program gives users an accurate edge identification application and a procedure for sampling improvement and ESF construction, Line Spread Function computation and MTF determination and plotting with the possibility of changing input data such as region of interest (ROI) dimensions (m lines, n pixels) and pixel size (display monitor). The output data can be directly displayed or saved in Excel formats. The most important functions of this program are:

1. Edge Identification: The initial task in MTF measurement is the identification of suitable edges for analysis. According to detection pixels grid vertical or horizontal axes, the edge must be oriented with a minimum tilt angle for an along scan or cross scan MTF determination (Figure 2). This minimum angle is required as well as sufficient length for suitable ESF construction (Kohm, 2004). It can be easily proven that at least two horizontal pixels should go through along the target edge to guarantee that sub-pixels will be placed on uniform grid after projection for ESF construction (Figure 2). In our case, the target length is 4.5 cm (~240 pixels), thus the minimum required angle is 0.47°. As the orientation of the angle changes, the resolution varies also, becoming either coarser or finer. The candidate edge must also meet contrast and noise requirements for selection (Jain, 1989). This is because, the MTF value obtained with high contrast edge target is always

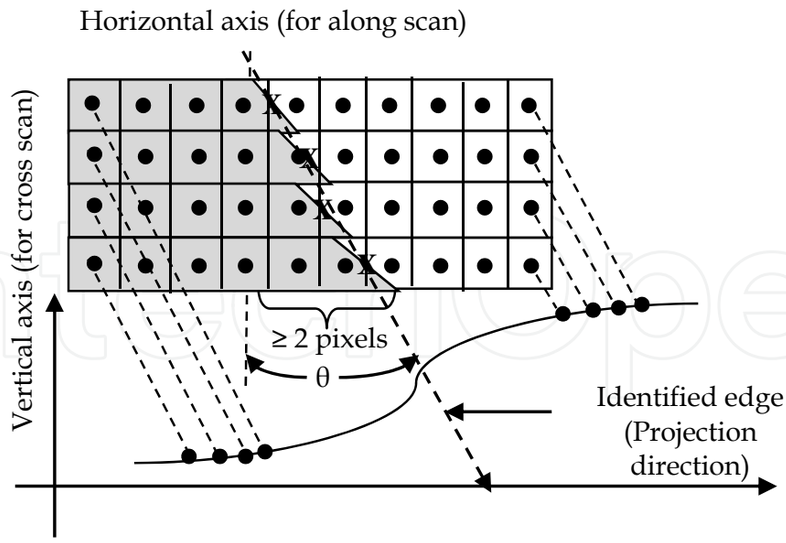

Fig. 2. Sampling improvement by profile line projection after edge identification (for clarity just first and last points are presented).

larger than that obtained with lower contrast target for a given spatial frequency; therefore, when the MTF of a system is presented, the contrast of the line pair used to measure the MTF should be given (Williams, 2004). In our case the maximum contrast of the target image obtained is 37.68% calculated by Michelson formula (Michelson, 1927). Noise can also affect contrast transfer and overall detection capability of imaging system. Therefore, the measured MTF by the used slanted edge method will be biased. The use of multiple lines of profile (m lines) for data improving can reduce the source of error but will usually not eliminate it completely (Burns, 2000). For practical purpose, different tilt angles (θ) varying from 1° to 5° were tested allowing relatively high and low resolution ESF generation. Before starting using our program for edge identification and MTF establishment, a Sobel edge detection operator followed by thresholding and binary morphological processing (filtering) is used to identify edge with the proper (real) orientation (θ_p) for a verification purpose (Figure 3). A value of θ_p of 0.95° was found for a tested tilt angle (θ) of 1° that prove the good target fixing and correct geometrical exposure conditions. After this verification, the image of the target obtained is first read and displayed in a suitable format (.bmp) by the developed program. The edge locations were accurately determined for each lines of profile of the selected ROI. An initial estimate of the location and angle of the edge is then determined by performing a least squares regression of selected points along the edge. The approximate equation of the identified edge average straight line is given by:

$$Y = ax + b \tag{1}$$

With:

$$a = \frac{\left(\sum_{i=1}^{m} x_i y_i\right) - \left(\sum_{i=1}^{m} x_i\right)\left(\sum_{i=1}^{m} y_i\right)}{m\left(\sum_{i=1}^{m} x_i^2\right) - \left(\sum_{i=1}^{m} x_i\right)^2}, \quad b = \frac{\left(\sum_{i=1}^{m} x_i^2\right)\left(\sum_{i=1}^{m} y_i\right) - \left(\sum_{i=1}^{m} x_i\right)\left(\sum_{i=1}^{m} x_i y_i\right)}{m\left(\sum_{i=1}^{m} x_i^2\right) - \left(\sum_{i=1}^{m} x_i\right)^2} \tag{2}$$

Where:
m = number of data (line number of the selected ROI);
X_i = row number;
Y_i = sub-pixel edge position.

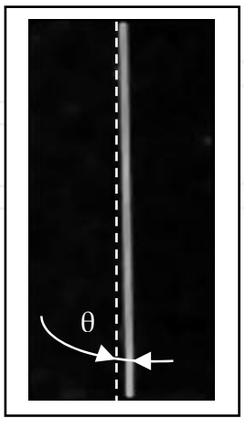

Fig. 3. Result of Sobel edge detection operator followed by thresholding and binary morphological processing (filtering) to identify the proper edge orientation (θ_p~0.95°, for θ=1°).

2. Sampling improvement and Edge Spread Function Construction: The ESF is the system response to the input of an ideal edge. As the output of the system is a sampled image, the fidelity of the edge spread function using a single line of image data is insufficient for MTF analysis. Aliasing due to under sampling in the camera, along with phase effects and the angle of the actual edge with respect to the sampling grid will cause variable results for a single line. The phase effects and edge angle may be exploited, however, to provide a high fidelity measurement of the ESF. Construction of the ESF is graphically represented in Figure 2. The edge is identified in the image as described above. A line is then constructed perpendicular to the edge. For a given line of image data, each point around the edge transition is projected onto the perpendicular line. This process is then repeated for each subsequent line of image data along the edge. The difference in sub-pixel location of the edge with respect to the sampling grid for different lines in the image results in differences in the location of the projected data point onto the perpendicular. This yields a high fidelity representation of the system response to an edge. Small changes in the edge angle used during construction of the super-sampled edge affect the quality of the resulting ESF. The angle is systematically adjusted by small increments of 0.25° around the initial estimate (5°) which is equivalent to one pixel shift of one edge extremity in left or right direction for an along scan. The resulting curve fit (equation) is used to refine the edge angle estimate for the final ESF construction. After the individual ESF data points have been determined, the data must be conditioned and re-sampled to a fixed interval. In general, the angle of the edge with respect to the sampling grid does not produce uniformly distributed data points along the perpendicular to the edge. Also, with longer edges, many data points may be located in close proximity to one another. Suitable 3 order polynomial data fitting is used to re-sample the data to uniformly spaced sample points. More sophisticated fitting algorithm is presented in reference (Cleveland, 1985).

To avoid data interference when performing projection operation, it is important that the selected tilt angle θ (projection angle) obeys the following condition:

$$an\ \theta \geq \frac{P_w}{N_{pl}P_h} \quad (3)$$

Where: P_w is the detected pixel width, P_h is the detected pixel height and N_{pl} is the number of selected profile lines.

The slanted-edge target used is a 25 µm thick foil of Gadolinium which is a highly neutron absorbing material allowing the production of suitable images with the necessary contrast between dark and light parts (edge). The used tilt angles are: 1° for the Sobel edge detection test and 5° for the MTF determination. To check the dependence between tilt angle and MTF result, some others target tilt angles, of values less than 10°, were tested.

The main characteristics of the neutron imaging system studied are presented in the following table (table.1).

Detector element	Sony ICX419ALL, ½ inch interline transfer CCD image sensor
Number of pixels	752(H) x 582 (V), 512x512 used
Unit cell size	8.6 µm x 8.3 µm
Minimum illumination	0.00002 lx. F1.4
Shutter speed or frames rate	Hi: 1/50, 1/125, 1/250, 1/500, 1/1000, 1/2000 sec
	LO: 1, 2, 4, 8 , 16, 32, 64, 128, 256 frame(s)
Manual gain control	8-38 dB
Dynamic range	Relatively Wide at standard imaging conditions
Bit depth	8 bits (255 levels)
Neutron Scintillator	250 µm LiF –ZnS, green emission (~520nm)
Mirror	Front-surfaced Al/SiO_2-mirror; optical flatness 2λ/25mm; reflectivity 94%
Signal to noise ratio	52 dB

Table 1. Main characteristics of the neutron imaging system studied.

Neutron radiography image were captured at the neutron radiograph facility of Es-Salam research reactor under neutron beam intensity of $1.5x10^6$ n/cm²/s and with a collimation ratio (L/D) of ~125. The exposure time to the neutron beam was 15 seconds. Selected camera gain was 18 dB. After target image capture, the developed code performs the following operations for MTF computation and plotting:

1. Target image reading in suitable format:
2. ROI selection, 240 lines x110 pixels were chosen from the image of the target. The main criteria for ROI selection are: 1) the width (n pixels) of the ROI must perfectly cover the edge area; 2) the length of the ROI (m lines) should be selected as long as possible to ensure the reduction of noise and low-frequency MTF estimation errors.
3. Edge identification and estimation of the real tilt angle. Edge positions were determined on a line-by-line (ESFs) basis using pixel profile information. For each single blurred line of profile (ESF) a simple digital differentiation is applied to detect maximum slope. The sub-pixel edge points are determined by fitting a cubic polynomial equation to the edge data using four values around the maximum slope point. Then, the zero crossing location of the second derivative of the polynomial coefficients indicates the curve inflection point,

which is assumed as the sub-pixel edge location. Finally, all the ESFs sub-pixel edge locations are forced to be a straight line by assuming that the edge is a straight line. This is done by fitting a line through the sub-pixel edge locations obtained from the previous step and then declaring the actual edge locations to be on the line. The least-squares approach for finding a straight line involves determining the best approximating line when the squared error of the sum of squares of the differences between the edge points on the approximating line and the given edge point values is minimized. All these operations are performed automatically by the developed program

4. Sampling improvement by determination of sub-sampling factor and ESF generation using data projection technique on an orthogonal line to the detected edge. Before data projection, the aligned edge data of every line of profile (ESF) taken from the ROI of the image target is interpolated with a cubic splines. Then all the ESFs are splined using the function spline.m of MATLAB. And finally, the averaged of splined ESFs is determined;
5. ESF data selection between 10% and 90% around edge area in the interval between maximum and minimum gray levels values (Fig.6 (b)) to avoid unnecessary frequencies considering when applying FFT;
6. Fitting a 3 order polynomial equation to average ESF data;
7. Numerical differentiation of fitted ESF curve allowing the determination of LSF;
8. Fast Fourier Transform of LSF with the application of Hamming FFT-window;
9. MTF plotting after normalization of FFT magnitude.

2.1.2 Example of practical application and experimental results

In order to characterize the imaging system being studied, the proposed procedure and developed code were used. The effective spatial resolution was determined for a recommended MTF value of 0.1 (*MTF10*). MTF10 is a value corresponding to the average human eye's separation power (resolution). Another very interesting MTF characteristic is MTF50 corresponding to a value of 0.5 of MTF (Nyquist Frequency) that provides the limit between an under-sampled and poor displayed image (very low frequencies) and an optimally sampled and well-displayed image (medium and high frequencies). The neutron image obtained of the examined edge target is shown in figure 4. Figure 5 represents the main window (screen shot) of the developed program used for MTF computation. The spatial resolution limit (R_l) of our system is calculated in mm by the following expression:

$$R_l = \frac{1[\mathrm{lp}]}{2\ \mathrm{MTF10}[\frac{\mathrm{lp}}{\mathrm{mm}}]} \tag{4}$$

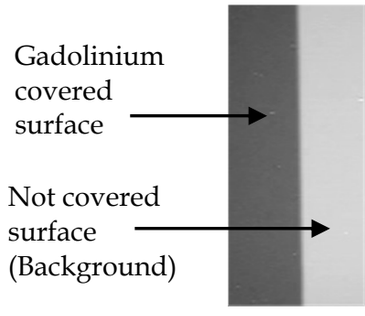

Fig. 4. Target neutron radiograph.

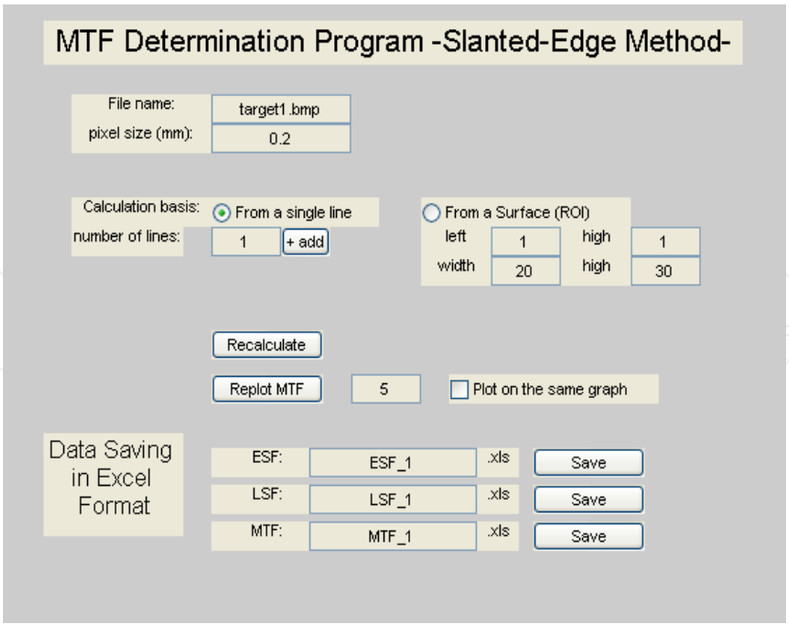

Fig. 5. Screen shot of the developed MatLab program (code).

Results for the main steps of MTF determination performed by the developed program such as edge identification, profile line superposition and interpolation (ESFs) and data projection by SPLINE function are presented in figures 6(a) and 6(b).

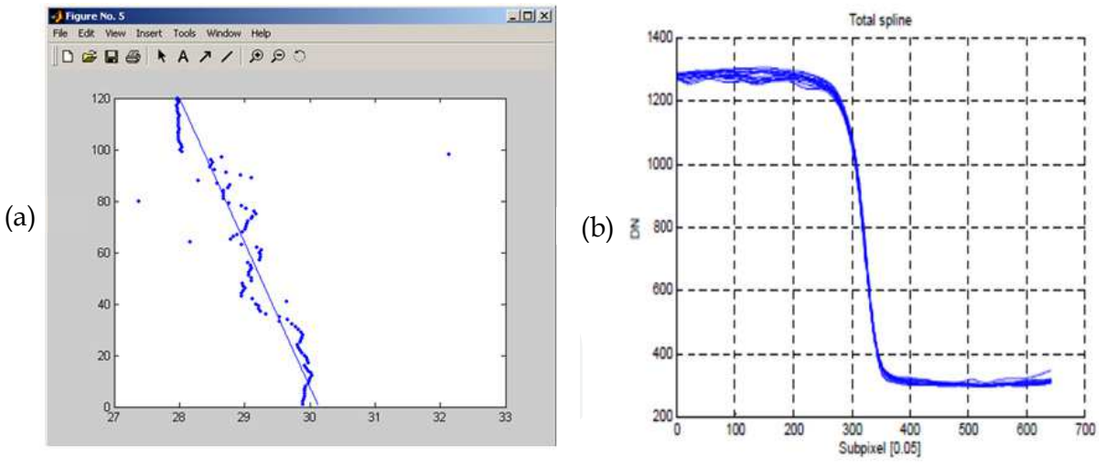

Fig. 6. (a) Example of edge identification by the developed code: after original image pixel decomposing into small intervals (polynomial fit steps), accurate edge location is detected in each horizontal line of profile across the edge and an average straight line of all detected locations is determined (least-squares) allowing thus data projection to improve ESF sampling (SPline), (b) Superposed profile lines using SPLINE function of MatLab.

Finally, the proposed code plots the MTF of the studied imaging system (Figure 7). The analysis of this MTF curve allows the characterization of spatial response of this system and the determination of spatial resolution limit.

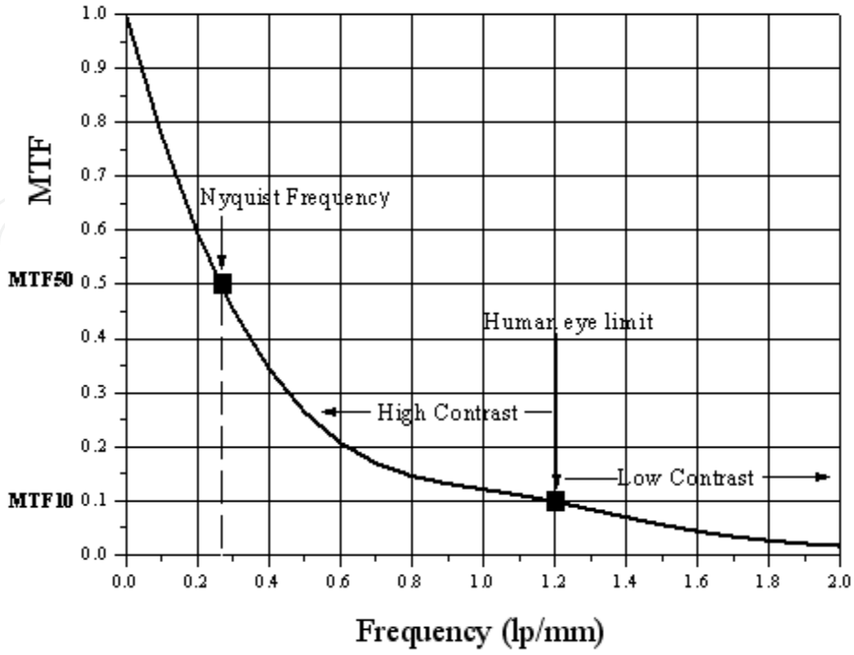

Fig. 7. MTF of the studied neutron imaging system.

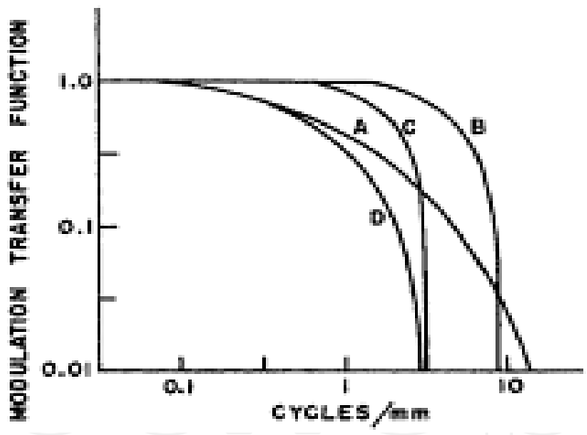

Fig. 8. MTF curves for components of a radiographic imaging system and the composite MTF for the entire system introduced for comparison purpose. A: MTF for the screen-film combination, B: MTF for a 1 mm focal spot with 90 cm between the focal spot and the object and 10 cm between object and film, C: MTF for 0.3 mm motion of the object during exposure, D: Composite MTF for the entire imaging system (Hendee & Ritlenour 2002).

When critically examining the obtained MTF, the following remarks and conclusions can be drawn:

1. The interesting and best exploited region of MTF is in the interval between the Nyquist frequency and the human eye's resolution. We can see that the MTF curve obtained

drop rapidly in this region. This is not a good characteristic of the imaging system studied because it allows a fair contrast image display when compared to other imaging systems with MTF dropping gradually (Figure 8). The CCD camera, in such a case, presents optimum separation ability (resolution) and, in term of gray levels (contrast), it reproduces fairly the image of the target.

2. The spatial resolution limit at MTF10 that correspond to an MTF of 0.1 is equal to 1.2 *lp*[1]*/mm*. This value is equivalent to 416 µm (according to equation 6) and is a very significant and an effective one because it is greater than the value of the intrinsic spatial resolution of ~200 µm of the studied imaging system. Deviation from the intrinsic resolution is due to many reasons and factors that are the following:
    1. The geometric properties of the neutron radiography facility: In our case, two parameters are dominant:
        a. The L/D neutron collimation ration (~125): for a practical case of Objetc-to-detector distance (L_f) of 5 cm, the induced geometrical Unsharpness ($Ug=L_f/(L/D)$ due to the beam spread when a point is projected at the same edge position is equal to 400µm.
        b. The scintillator thickness: for scintillator-based converter system, the first source of blur is spreading of emitted light within the scintillator material. The spreading is determined by the material's thickness and by the design of the scintillator in terms of its crystal structure and its neutron absorptive and light emission properties.

        Despite all these constraints, the geometric blurring can be minimized by reducing the object-to-image detector distance as much as possible (e.g., contact), and by increasing the collimator inlet aperture-to-object distance (L) to a suitable level not affecting the neutron beam intensity considerably.
    2. The imaging technique: indeed indirect-conversion method of the used image detector can scatter light over several pixels, further limiting the effective resolution of the system, more so than indicated by pixel size alone (intrinsic resolution).
    3. Optical properties: the intrinsic resolution can often be degraded by other factors which introduce blurring of the image, such as improper focusing and light reflection by the mirror.

However, one cannot isolate spatial resolution effects on neutron image quality from effects due to quantum mottle and electronic noise under typical digital image acquisition conditions.

2.2 Temporal resolution

2.2.1 Temporal resolution estimation

The temporal resolution is determined by the frame rate and by the exposure-time of the camera. These limit the maximal speed of dynamic events that can be well captured by the neutron camera. Rapid dynamic events that occur faster than the frame rate of CCD cameras are not visible (or else captured incorrectly) in the recorded video sequences. There are two typical visual effects in video sequences which are caused by very fast motion (Shechtman,

[1] *lp* : line pairs or cycle.

2005). One effect (motion blur) is caused by the exposure-time of the camera and the other effect (motion aliasing) is due to the temporal sub-sampling introduced by the frame rate of the camera. In our case of neutron imaging, only motion blur is of interest. It occurs when the camera integrates the light coming from the scene (scintillator) during the exposure time in order to generate each frame. As a result, fast moving objects produce a noted blur along their trajectory, often resulting in distorted or unrecognizable object shapes. The faster the object moves, the stronger this effect is, especially if the trajectory of the moving object is not linear (Shetchman et al., 2002). To quantify this motion blur and therefore to determine the temporal resolution limit, we proceed as follows: the neutron imaging video of a rotating cadmium indicator is captured for different rotational speeds (0.0017, 0.45, 1.2 and 1.65 RPS[2]) and different frame rates (Figure 9). The indicator used is a thin 7.9 mm wide cadmium blade. It was put into rotational motion by a speed controlled electrical motor. Video sequences (Vid. Seq.) for different indicator rotational speeds are captured under the following conditions (table 2):

	Frame rates (fps[3])	**Neutron beam intensity**	**Camera Gain**	**Exposure time (s)**
Vid. Seq.1	12.5	$1.5x10^6$ n/cm²/s	22 dB	90′
Vid. Seq.2	25	$1.5x10^6$ n/cm²/s	22 dB	90′
Vid. Seq.3	50	$1.5x10^6$ n/cm²/s	22 dB	90′
Vid. Seq.4	125	$1.5x10^6$ n/cm²/s	22 dB	90′
Vid. Seq.5	250	$1.5x10^6$ n/cm²/s	38 dB	90′

Table 2. Experimental video sequences capture conditions.

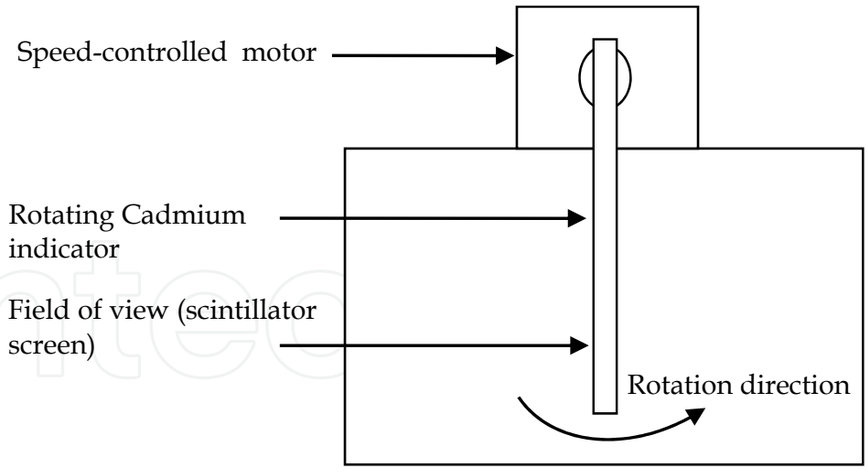

Fig. 9. Experimental arrangement for induced motion blurs characterisation.

The video sequences obtained are examined with suitable image processing and analysis software (Image J). The used CCD neutron camera integrates light coming from the scintillator screen during the exposure time in order to generate each frame. The software

[2] RPS : rounds per second.
[3] fps: frames per second.

enables the calculation of the motion blur B using equation (5) for each video sequence obtained. The motion blur in this case is considered as the width (in pixels) of the shade involved behind the rotating indicator appearing in each frame. This width is measured at the middle of the indication on a selected frame. The data obtained allows us to determine the effective limits of temporal resolution for each rotational speed.

$$B = I_{wi} - I_{wr}\left[\frac{L_f}{L}\left(1 - \frac{D}{I_{wr}}\right) + 1\right] \quad (5)$$

where: I_{wr} is the real indicator width (7.9mm), I_{wi} is the indicator width measured on the obtained image, L_f is the distance between the indicator position and the scintillator screen (10.5 mm), L is the distance between the collimator inlet aperture and the indicator position (2500.5 mm), D is the collimator inlet aperture diameter (20 mm).

2.2.2 Experimental results

Selected frame from captured video sequences is presented in figure 10. Preliminary analysis of the video sequences obtained shows that the temporal resolution is affected principally by motion blur and not by motion-based aliasing.

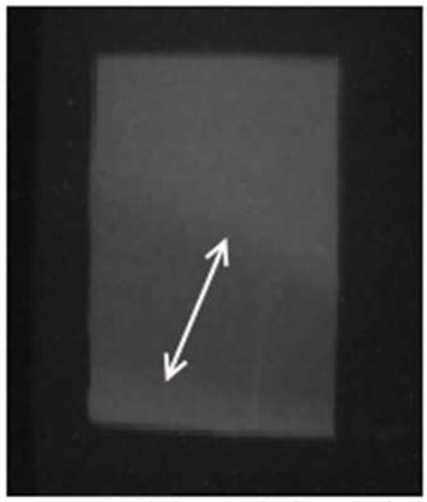

Fig. 10. Selected frame showing the indicator position and motion blur width taken from selected video sequence captured with a frame rates of 12.5 fps and for a cadmium indicator's rotation speed of 0.45 RPS.

Motions blur variation as a function of frame rate is presented in figure 11. Graphs 1 and 2 correspond to indication rotation speeds of 0.45 and 1.2 RPS respectively.

On graphs 1 and 2, we can easily verify that motion blur decrease when the frame rate is increased up to critical values where it became constant. It was observed that the critical points are located at 12.5, 50, 125 and 250 fps on the frame rate axis for, respectively, 0.0017, 0.45, 1.2 and 1.65 RPS of the cadmium indicator rotation speeds. These critical points correspond to the temporal resolution limits that retain motion blur at a minimum although with low image dynamic range. Results of temporal resolution limits for different rotational speeds are shown in figure 12.

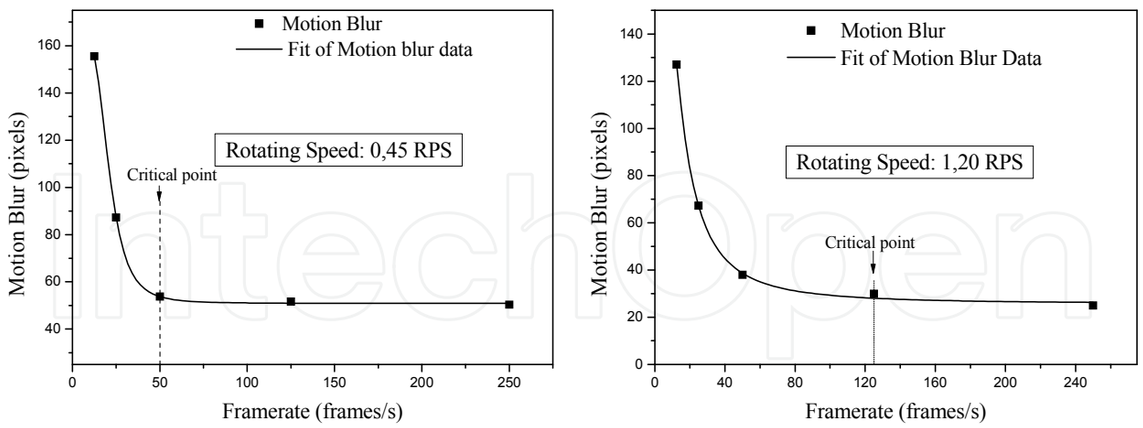

Fig. 11. Motion blurs variation of video sequences in function of frame rates for two rotation speeds of the cadmium indicator.

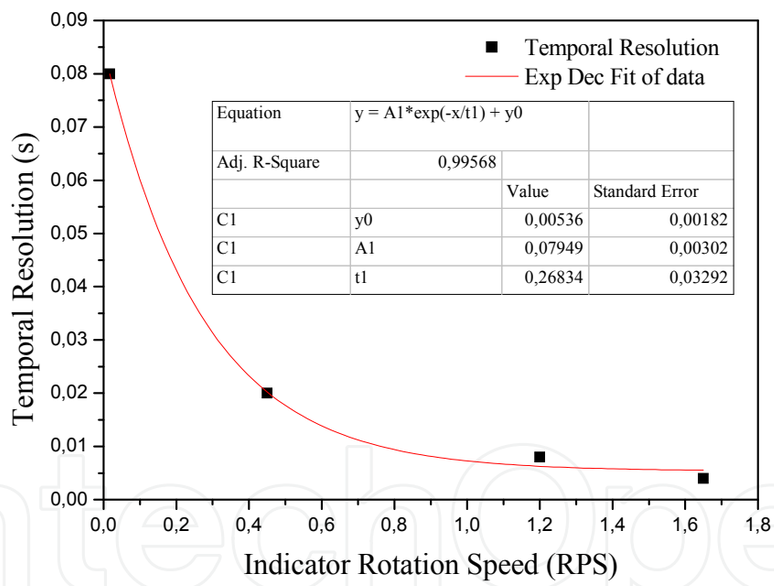

Fig. 12. Temporal resolution limits as a function of indicator rotation speed. The temporal resolution limit allowing optimum image quality in term of motion blur, with, certainly a low dynamic range, presented in this figure are for specific exposure and image capture conditions, namely: a neutron beam intensity of 1.5×10^6 n/cm^2/s, a camera signal gain of 22 dB and 38 dB (last point).

As we can see in figure 11, the temporal resolution limit is closely related to the indicator rotational speed. These values give an idea about the optimal frame rate that must be selected to avoid motion blur but not necessarily the most suitable for optimum frame exposure. With low frame exposure contrast and dynamic range can be seriously affected

especially when the neutron beam intensity is low. Finally, it's very important to mention that the video sequence captured are, relatively, not rich in terms of gray levels digitalization and contrast because of the limited dynamic range and bit depth (8 bits) of the imaging system being studied. In this work, it is obvious that, the image quality is analyzed and judged regarding to the performance of the imaging system used for neutron video capture. In order to improve the video image quality it is recommended to increase the neutron beam intensity at the sample level to the maximum and to use a CCD camera with a high bit depth (+14 bits).

3. Criteria for best video capture results and application of super resolution in neutron imaging

Dynamic process imaging using a neutron beam is a very powerful and interesting investigative tool as far as light materials, elements and substances such hydrogen, water lubricants and some other relevant materials are concerned. The neutron imaging system that is most utilised is based on a CCD camera (charged coupled device) and scintillator screen. Because of the complexity and large number of operations necessary for capturing dynamic processes with any neutron digital imaging system (neutron camera), specific optimum experimental conditions and procedural accuracy are required. The sequence of events required to capture a single image with a full-frame CCD camera system is summarized in reference (SIT Technical Note, 1994).

In neutron imaging with CCD-based neutron camera, there are several camera operating parameters that modify the readout stage of image acquisition and have an impact on image quality (Spring, K. R. et al., www.microscopyu.com/articles/digitalimaging/ccdintro.html). The two most important ones are the frame rate (FRM) and the gain (G). The frame rate (also referred to as the readout rate) of most scientific-grade CCD cameras is adjustable. The maximum achievable rate is a function of the processing speed of the camera electronics, which reflects the time required to digitize a single pixel. Applications aimed at tracking rapid kinetic processes require fast readout and frame rates (FRM) in order to achieve adequate temporal resolution. In certain situations, a video rate of 30 frames per second or higher is necessary. A second camera acquisition factor, which can affect image quality because it modifies the CCD readout process, is the electronic gain (G) of the camera system. The gain adjustment of a digital CCD camera system defines the number of accumulated photoelectrons that determine each gray level step distinguished by the readout electronics, and is typically applied at the analogue-to-digital conversion step.

In this work, video sequence quality in terms of contrast, resolution and noise are studied and the most suitable conditions for the flow process examination are determined as a function of the neutron beam intensity. The second objective of this work is the application of a post acquisition super resolution (SR) processing procedures to improve the quality of the neutron video obtained. The neutron imaging system used is the same as described before.

3.1 Neutron video capture conditions study

According to previous work results, it was demonstrated that the optimum acquisition parameters for a water flow process capture are respectively: 12.5 fps as a capture frame rate

(display 29.97 fps, MPEG-1 format) and a selected value of 22dB as a signal gain for the case of the imaging system being used (Kharfi et al, 2011). In this work the captured video images have been analyzed in terms of contrast, noise and resolution according to the neutron beam intensity. This is to check the effect of the neutron beam intensity on the image quality. The quantification of contrast, noise and resolution of the neutron video captured is based on histogram and edge profile analysis. Indeed, understanding image histograms is probably the single most important element in the analysis of images or video sequences from a digital CCD camera. A histogram can tell us whether or not the image has been properly exposed, and what adjustments will work best. Noise is the most important variable that can strongly affect the quality of a digital image or video. In this work, only gamma radiation noise (impulse noise) that appears in images as undesirable white spots is considered. The gamma noise can be estimated through the statistical measure called the "standard deviation," which quantifies the typical variation that a pixel gray-scale value will have from its mean and "true" value. This concept can also be understood by looking at the histogram for a carefully selected bright region of interest (ROI) on a frame arbitrarily selected from the video sequence obtained.

A histogram can also describe the amount of contrast. Contrast is the difference in brightness between light and dark areas in a frame. In this work, the maximum contrast is estimated according to Michelson formula given by Eq.5 (Michelson, 1927):

$$C = \frac{I_{max} - I_{min}}{I_{max} + I_{min}} \tag{6}$$

with I_{max} and I_{min} representing the highest and lowest luminance of the analyzed image.

In neutron imaging, it is common that not all important image quality criteria can be simultaneously optimized in a single image, or a video. Obtaining the best images within the constraints imposed by a particular process or experiment typically requires a compromise between the listed criteria, which often exert contradictory demands (Anderson, 2009). In order to study the influence of the neutron beam intensity on the neutron video quality, capture of time-lapse sequences of water and car engine oil flows inside a metallic container system is performed. Several videos are captured under different experimental neutron exposure conditions of the flow process. Details and conditions of video sequences capture are shown in table 3. The experiment setup used consists of two Aluminium compartments which communicate through three holes of 1mm, 1.5 mm and 2 mm in diameters (figure 13).

	Liquid	**Neutron beam intensity (n/cm²/s)**	**Gain (dB)**	**Capture frame rate (fps)**
Video Sequence.1	water	1.6×10^6	22	12.5
Video Sequence.2	water	1.44×10^7	22	12.5
Video Sequence.3	car engine oil	1.6×10^6	22	12.5
Video Sequence.4	car engine oil	4.8×10^6	22	12.5
Video Sequence.5	car engine oil	9.6×10^6	22	12.5
Video Sequence.6	car engine oil	1.44×10^7	22	12.5

Table 3. Experimental video sequences neutron exposure and capture conditions.

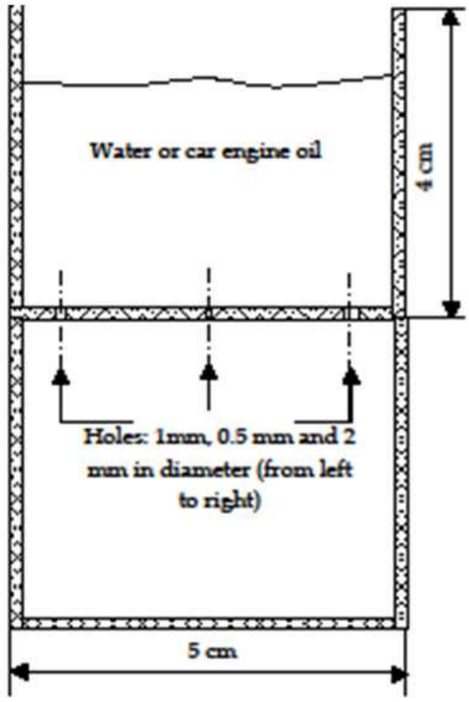

Fig. 13. Experimental system used in the study and visualization of water and car engine oil flow process through three different diameter holes.

3.2 Super resolution video sequence enhancement procedures and algorithms

Super resolution (SR) is a mean of producing a high-resolution (HR) image from one or a set of low-resolution, blurred and noisy images. It represent the capacity to transform noisy and blurred images obtained by low resolution (LR) imaging system (camera) to a higher resolution (HR) image with greater details than those of LR image. Methods of SR are classified coarsely into two categories: (1) The classical multi-images super resolution methods, and (2) Example based super resolution (Irani et al., 1991, Capel, 2004, Farsiu et al., 2004). Practically, classical methods allow small increases in resolution by factor smaller than two (Baker et al., 2002). However, example-based SR methods have been shown to exceed the limits of classical methods (Freeman et al., 2000, Kim et al., 2008). Other more sophisticated methods for image up-scaling based on learning edge models have also been developed and proposed (Sun et al., 2008). To achieve this HR image with classical multi-image super resolution methods, usually, an estimation of an image which minimizes the difference between its projection and each of the low resolution (LR) images through suitable algorithms is performed based on iteration process. LR images must have different sub pixel shifts, so that every image contains new information. To guarantee this last condition, two alternatives are available: 1. Extracting a number of frames from a video that are captured in a very small laps of time, 2. camera is moved from frame to frame, 3. multiple cameras are used in different positions. SR restores HR images from degraded (noisy, blurred and aliased) images. The first step in SR procedure application is the formulation of a model that relates between HR image and LR image. The common used model is given by the following equation (Sroubek & Flusser, 2007, Sung et al., 2003):

$$y_k = D_k B_k M_k x + n_k \quad (7)$$

Where:
- M_k is the Warp matrix (Translation, Rotation);
- B_k is the Blur matrix ;
- D_k is the Sub sampling matrix;
- n_k is the noise vector ;
- x is the original HR image;
- y_k is the observed LR image.

With this simple formulation, the direct solution estimate can be inaccurate. Robust SR methods can help to improve this solution. The solution estimate in each iteration is updated by a gradient iterative minimization method given by the following expression:

$$x^{n+1} = x^n + \delta \nabla E(x) \quad (8)$$

where $E(x)$ is the total squared error of resampling the high-resolution image represented by x and δ is a scale factor defining the step size in the direction of the gradient.

$$E(x) = \frac{1}{2}\sum_{k=1}^{n} \| y_k - D B_k M_k x \|_2^2 \quad (9)$$

The gradient of x is can be given by:

$$\nabla E(x) = \sum_{k=1}^{n} B_k \quad (10)$$

Robustness is introduced by replacing this last sum of images by the scaled pixel median:

$$\nabla E(x) = n.median\{B_k\}_{k=1}^{n} \quad (11)$$

Some other combinations in addition to the median operator can also be applied to get more suitable and accurate results.

The procedure of SR consists of three stages (Fig.14):

1. registration;
2. interpolation onto HR grid;
3. Removing blur and noise.

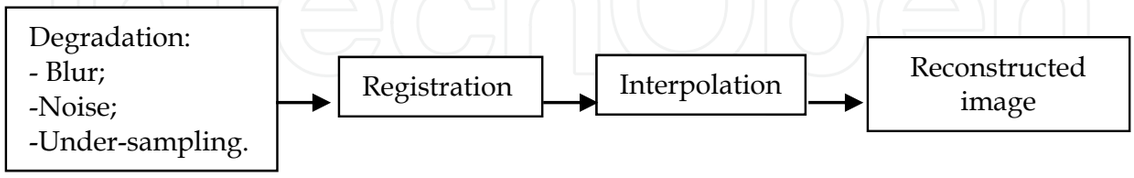

Fig. 14. Model for Super Resolution for observed LR.

The most important SR image reconstruction approaches are the following:

- Non uniform interpolation approach;
- Frequency domain approach;
- regularized SR reconstruction approach;
- Projection onto convex sets approach;

- Maximum likelihood projection onto convex sets hybrid reconstruction approach;
- Iterative back-projection approach.

The second objective of this work is the application and testing of SR procedure based on robust method on a neutron imaging video in order to improve their quality in term of spatial resolution by reducing the motion blur and also in term of noise. For such a purpose, we have adapted a Robust SR procedure described in (Zomet et al., 2001) in a MATLAB code to improve the quality and resolution of neutron video obtained. This method is an Iterated Back Projection one that computes the gradient, which is not given by the sum of all errors, but by the median of all errors. This brings robustness against outliners in the LR images.

For practical purpose, the video frames are, first, rearranged into sets of frames (5 frames in each one). Then, the SR procedure mentioned above is applied on each set of frames separately with an interpolation factor of 2 (figure 15). For each set of frame, the motion

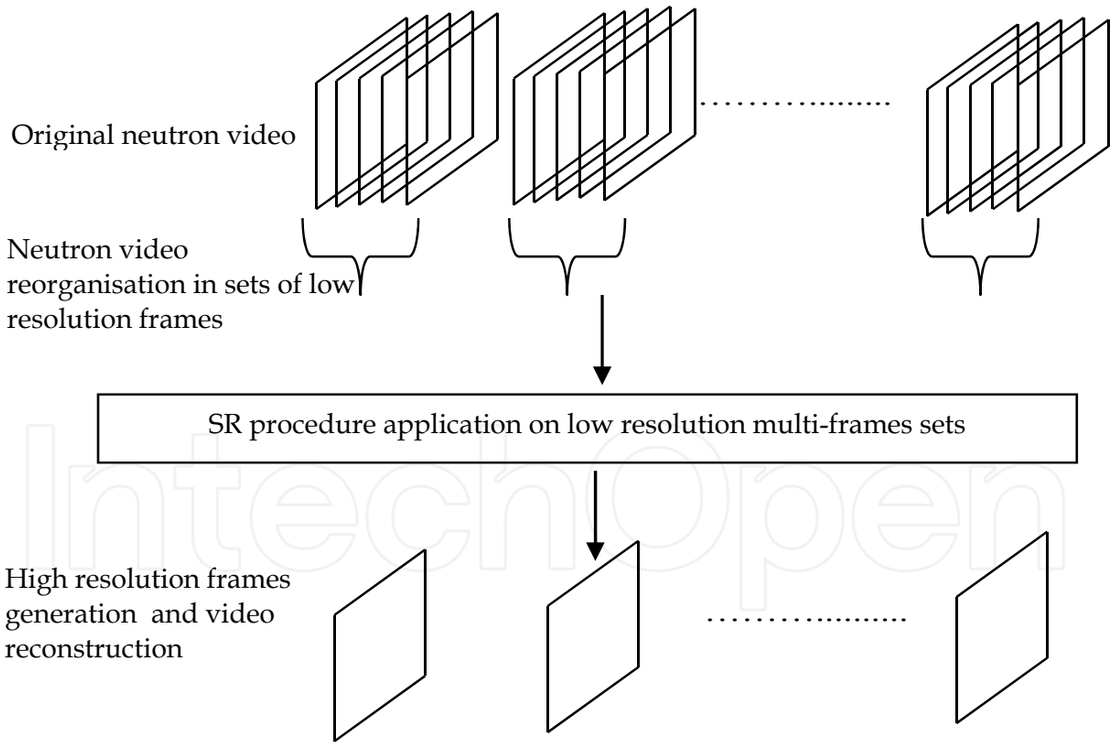

Fig. 15. Neutron video reorganisation in sets of multi-frames, SR procedure application on low resolution frames, high resolution frames generation and high resolution neutron video reconstruction.

estimation that is necessary for the application of this SR method is performed with Vandewalle et al (2006) algorithm. This method uses the property that a shift in the space domain is translated into a linear shift in the phase of the image's Fourier Transform. Similarly, a rotation in the space domain is visible in the amplitude of the Fourier Transform. Hence, the Vandewalle et al. motion estimation algorithm computes the images' Fourier Transforms and determines the 1-D shifts in both their amplitudes and phases. One advantage of this method is that it discards high-frequency components, where aliasing may have occurred, in order to be more robust. When all the frames sets are processed, the HR frames generated are used for a high resolution neutron video reconstruction and displaying with a standard speed of 25 fps or 30 fps (figure 14). To guarantee a best result with this proposed procedure, the capture frame rate of the examined dynamic process must be higher than the displaying one which is generally selected equal to 25 or 30 fps, depending on the used standard. The robust method applied to improve spatial resolution is based on pixel interpolation and super-sampling. The presented example in this chapter will not claim for completeness. The field of neutron imaging is experimental and seems to change with every new system built and CCD camera used for the examinations.

It is very important to mention that the capture frame rate must be accuracy selected to guarantee the optimum exposure of each frame to the neutron beam that is necessary for the well perception of the dynamic process being examined regarding its speed. The spatial resolution limit of the imaging system must be also taken into consideration. In our case the selected video capturing speed (frame rate) of 12.5 fps is sufficient to ensure the optimum visualization of the studied dynamic process. The rearrangement of the obtained video into frames sets of 5 frames doesn't affect the video quality. This is because our imaging system has a spatial resolution limit of ~ 400 μm and the average speed of the studied flow is about 0.095 m/s. According to these data, the equivalent video frame rate after SR procedure application, which is equal to the ratio of the average speed and the spatial resolution limit values, is approximately equal to ~2.35 fps. This effective frame rate when multiplied by 5 must give a value that is in the order of the selected video capture frame rate of 12.5 fps (5x2.35=11.75). Indeed, the selected capture frame rate and the number of frames in each set ensure the optimum visualization of studied flow process.

3.3 Results and discussions

3.3.1 Best video capture practical conditions establishment

Selected frames from the video sequences obtained are presented in figure 16 and 17. Selected region of interest (ROI) of 40x30 pixels are indicated by dashed and white squares. These regions indicate where gray levels measurements are performed that allow the calculation of necessary standard deviation for the estimation of noise and the necessary maximum and minimum gray levels values for the determination of contrast. A summary of the results obtained is given in table 4 based on histogram analysis. The variation of contrast and noise as a function of neutron beam intensity is shown in figure 18(a) and 18(b).

From the results obtained, we can first observe that at the maximum neutron beam intensity of 1.44 x 10^7 n/cm^2/s, the video sequence obtained is the best one in terms of contrast and

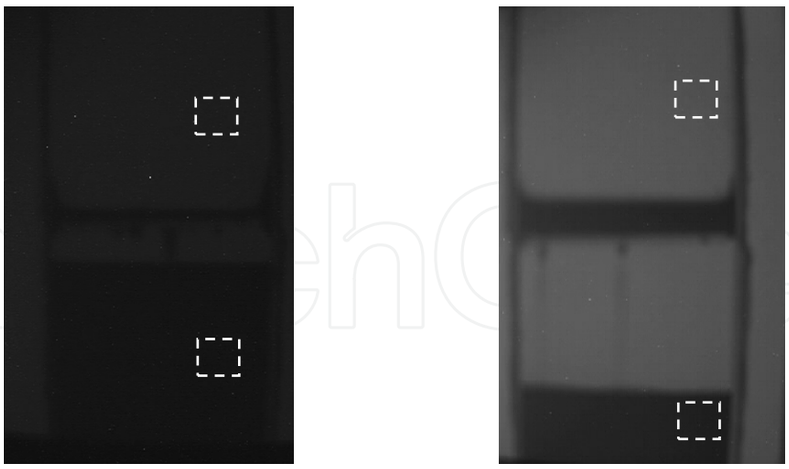

Fig. 16. Frames taken respectively from video sequence 1 and 2 of the water flow process for a frame rate of 12.5 fps, a Gain of 22 dB and a respectively neutron beam intensity of 1.6 x 10^6 n/cm^2/s and 1.44 x 10^7 n/cm^2/s (from the left).

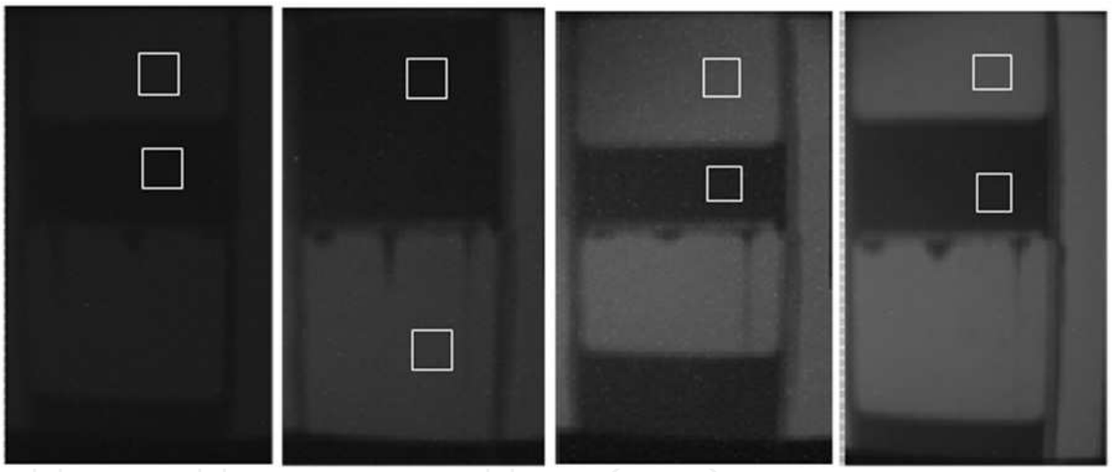

Fig. 17. Frames taken respectively from video sequence 3, 4, 5 and 6 of the car engine oil flow process for a frame rate of 12.5 fps, a Gain of 22 dB and a respectively neutron beam intensity of 1.6 x 10^6 n/cm^2/s, 4.8 x 10^6 n/cm^2/s, 9.6 x 10^6 n/cm^2/s and 1.44 x 10^7 n/cm^2/s (from the left to the right).

Video Sequences	liquid	Thermal noise (std.dev)	Contrast
Video Sequence.1	water	1.58	0.184
Video Sequence.2	water	1.52	0.409
Video Sequence.3	car engine oil	1.35	0.164
Video Sequence.4	car engine oil	2.35	0.376
Video Sequence.5	car engine oil	4.05	0.426
Video Sequence.6	car engine oil	1.89	0.446

Table 4. Summary of results obtained.

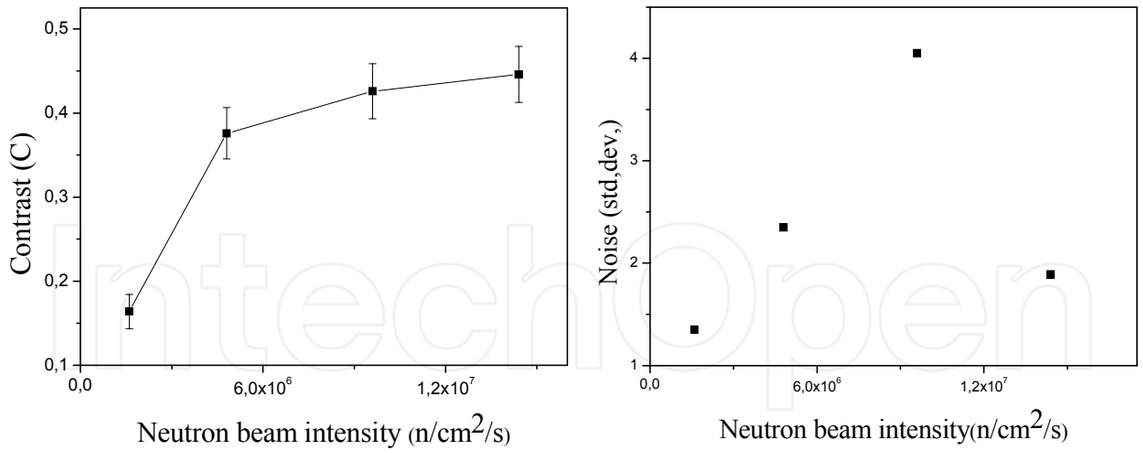

Fig. 18. (a: left). Contrast variation as a function of neutron beam intensity, (b: right). Random distribution of noise as a function of neutron beam intensity.

noise. Thus, a value of a neutron beam intensity of 1.6 x 10^6 n/cm²/s is not enough to produce a well perceptible neutron image with a wide dynamic range in this case of studied flow process. The contrast was found proportional to the neutron beam intensity but after a value of ~ 1x10^7 n/cm²/s it becomes almost constant (kharfi et al., 2011). The impulse noise that affects the video sequences has a random distribution as a function of the neutron beam intensity. The optimum exposure and acquisition parameters that allow capturing a high quality neutron video sequence for this case of flow process examination are the following (table 5):

parameters	Neutron beam intensity	Capture Frame rate	Gain
Optimum value	1x10^7 n/cm²/s	12.5 fps	22 dB

Table 5. Optimum video capture parameters.

In this work, it was established that the best video sequences 2 (water) and 6 (oil)) were obtained with a frame rate of 12.5 fps and a gain of 22 dB for a neutron beam intensity 1.44 x 10^7 n/cm²/s. These exposure and capture video condition have guaranteed 256 digitized levels (full dynamic range). These video sequence are well exposed, the different phases of the flow process (continuous flow, drops) are well perceptible. These video can be well exploited in study the flow process phases and the drops shape as a function of hole diameter. The flow speed as a function of pressure and hole diameter can be also measured. Thus, the neutron video sequences obtained are rich in information and can be used for a wide variety of applications and purposes in the domain of fluid flow analysis. A future works will be focused on the exploitation of such video sequence information for a specific flow analysis.

3.3.2 Practical example of video capture and Super Resolution image quality improvement

According to the above results, video sequence 5 captured at a neutron beam intensity of 4.8 x10^6 n/cm²/s is the highly noised one. A selected LR frames set is taken from this video sequence. A frame from this set is shown in figure 19 with its corresponding FFT[4] and

[4] FFT : Fourier Fast Transform.

histogram. The FFT is used to show the frequency support of the noisy and low resolution original frame and the histogram can inform us about sampling, gray levels distribution and noise affecting this frame. The SR algorithm and method described above is applied with an interpolation factor of 2 to improve the quality of this frame after a shift estimation.

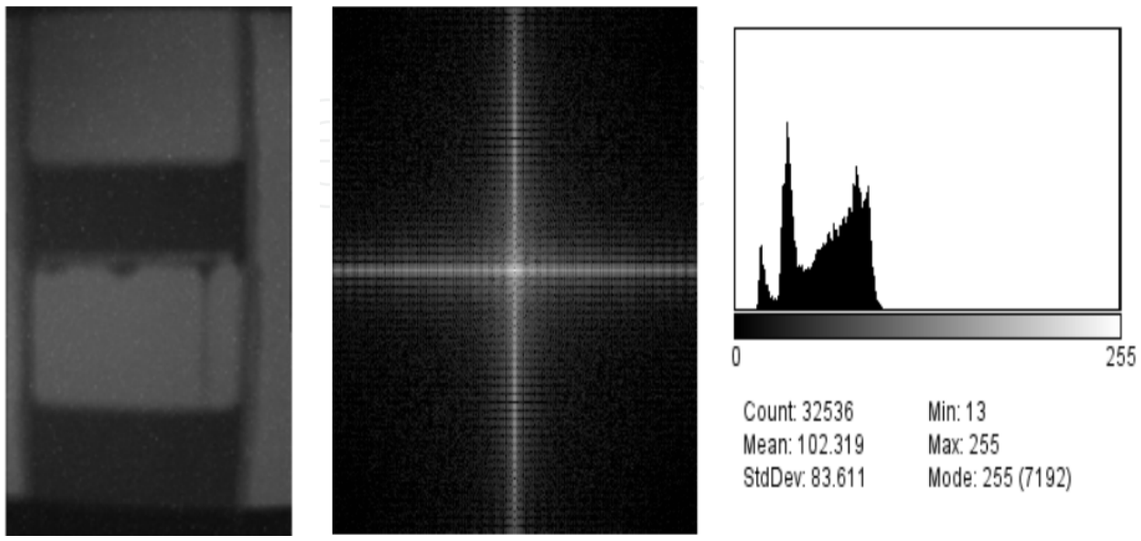

Fig. 19. One of the five LR frame selected from a set after arrangement of obtained neutron video in a number of frames sets and its corresponding FFT and histogram.

Example of generated high resolution frame result after the SR method application is shown in figure 20 with the corresponding FFT and histogram.

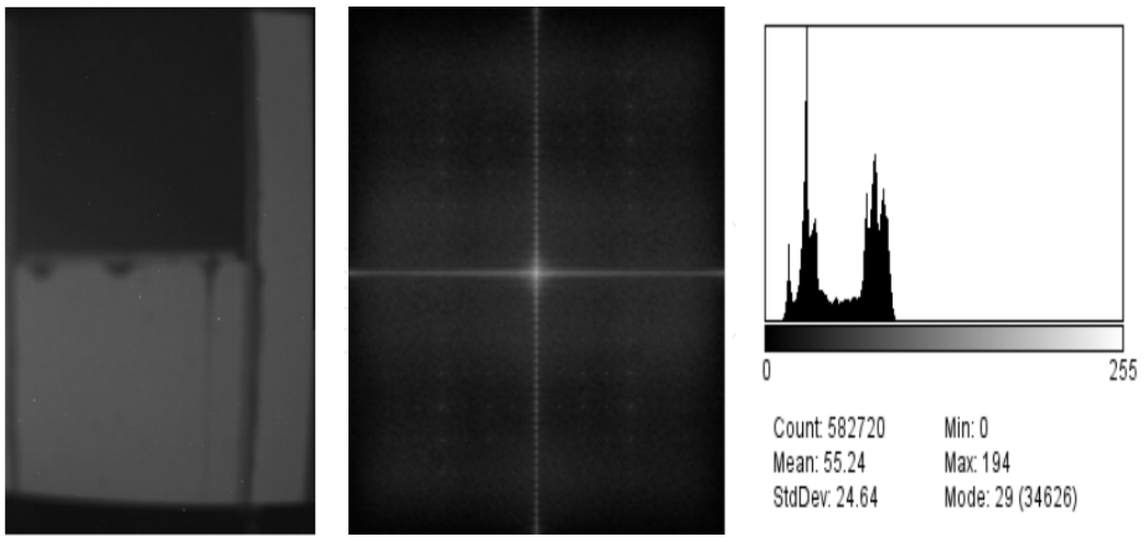

Fig. 20. Super resolved frame obtained after the application of the Robust Super resolution method on a set of low resolution frames arbitrary selected from the obtained neutron video of the flow process and its FFT and Histogram. When comparing FFT and histograms, we can easily verify that the sampling and resolution are improved and the noise (standard deviation) is significantly reduced.

From the HR frames obtained by SR procedure, a new high sampled and lowly noised neutron video is reconstructed. Although the neutron images (frames) processed through the proposed SR method are originally of optimum quality because a prior good selection of suitable video capture parameters was performed, the application of such SR method can reduce noise and improve the sampling of the obtained images and therefore allow the possibility to exploit theses images quantitatively. Because of the high sampling performance of the used CCD camera, not all SR methods are suitable for neuron images and video enhancement. The methods if well adapted and applied can contribute to improve the quality of neutron images and video suffering from motion blur with high efficiency.

4. Conclusions

Ultimately, the MTF is one component in characterizing the overall image quality performance of an imaging system. A robust method for estimating the MTF of high sensitivity neutron imaging CCD camera is presented. Longitudinal scan MTF results for the neutron imaging system are provided. Although the ISO 12233 slanted edge methodology was originally designed mostly for digital still camera MTF evaluation, it can successfully be applied to our neutron imaging system characterization. The weak dependence on tilt angle for values of less than 10° (the standard recommendation is 5°) allows the alignment constraints to be relaxed. The use of a standardized target and a specifically developed program allows MTF data to be easily and quickly obtained from a single target image. The ISO slanted-edge technique is seen to be a valuable alternative for fast and efficient MTF measurements, allowing the determination of spatial response and effective spatial resolution of the neutron imaging system being studied.

The approach followed and the experimental procedures for temporal resolution limit determination were found to be very suitable and allowed the production of very accurate data. Although, our neutron camera can operate under high frames rates, the temporal resolution is limited and cannot exceed some values which are conditioned by the intensity of the neutron source, the performance of the imaging system and the speed of the dynamic process under examination. The study of temporal resolution limits for the case of higher indicator's rotational speeds (1.2 and 1.65 RPS) demonstrates that, in order to get the best visualization conditions, the frame rate must be increased. Practical tests reveal that this last operation may cause contrast degradation and brightness loss in the frames of the neutron video produced. This, because of the limited dynamic range - due to the limited neutron beam intensity- and the small bit depth of the imaging system used.

Results of flow processes studied by imaging with our neutron imaging system demonstrate that different capture conditions situations often produce completely different neuron video results in terms of noise and contrast. A small number of CCD performance factors and camera operating parameters such as frame rate and signal gain dominate the major aspects of digital image quality in neutron imaging; and their effects overlap to a great extent. The neutron beam intensity was also demonstrated as an important exposure parameter that can modify completely the quality of neutron image in terms of contrast and dynamic range. A flux of ~ $1x10^7$ $b/cm^2/s$ was found enough to produce a high contrast image with a maximum dynamic range. For our case of flow process, frame rates of 12.5 fps with a signal gain of 22 dB were found as optimum video capture conditions. The super resolution method tested in this work proves that it is possible to improve the quality of the neutron

video sequence with a post processing procedures. Here it is very important to mention that the post processing procedures must be well selected to avoid unnecessary processing.

5. References

Crow, L. (2009). Neutron detectors for imaging. In: *Neutron imaging and applications* Anderson, I.S., McGreevy, L. M., Biheux, H. Z., pp.(47-66) , Springer Science, ISBN: 978-0-387-78692-6.

Baker, A., Kanade, T. (2002). Limits on super resolution and how to break them, *IEEE Transactions on Pattern Analysis and Machine Intelligence (PAMI)*, 24(9), pp.(1167-1183).

Burns, P.D. (2000). Slanted-Edge MTF for Digital Camera and Scanner Analysis, *Proc. IS&T 2000 PICS Conference*, pp. (135-138).

Capel, D.P. (2004) *Image mosaicing and super resolution*. Springer-Vergla, ISBN: 1852337710.

Cleveland, W. (1985). *The Elements of Graphics Data,* Ward Worth, Belmont, CA, USA.

Domanus, J.C. (1992). *Practical Neutron Radiography*, Kluwer Academic Publishers, Dordrecht, Holland.

Estribau, M., Magnau, P. (2004). Fast MTF measurement of CMOS images using ISO 12233 Slanted-edge methodology, *Proceedings of the Society of Photo-optical Instrumentation Engineers (SPIE), vol.5251*, 2004, pp.(243-252), Bellingham, WA, USA, ISBN:0-8194-5135-5.

Farsiu, S., Robinson, M.D., Elad, M., Milanfar, P. (2004). Fast and robust multiframe super resolution. *IEEE Transactions in image processing*, vol. 13, No 10, pp. (1327-1344).

Freeman, W.T., Pasztor, E., Carmichael, O.(2000). Learning low-level vision, *International Journal of Computer Vision (IJCV)*, 40, No.1, pp.(25-47), Kluwer Academic Publishers.

Hendee, W.R., Ritlenour, E.R. (2002). *Medical imaging physics*. Wiley-LISS, New York.

Irani, M., Peleg, S. (1991). Improving resolution by image registration. *Graphical Models and Image Processing*, 53, pp. (231-239).

Jain, A. (1989). *Fundamental of Digital Image Processing*, Prentice Hall, Englewood Cliffs, NJ, USA.

Jespers, P. G., Van de While, F., White, M. H. (1976). *Solid State Imaging,* Noordhoff International Publishing, pp. (485-522).

Kharfi, F., Abbaci,M., Boukerdja, L. Attari, K. (2005). Implementation of Neutron Tomography around the Algerian Es-Salam Research Reactor: preliminary study and first steps, *Nuclear Instrument and Methods in Physics Research, vol. A542*, pp. (213-218).

Kharfi, F., Denden, O., Ali, A. (2011). Implementation and characterisation of new neutron imaging system for dynamic processes investigation at the Es-Salam research reactor, *Journal of Applied Radiation and Isotopes*, 69, pp.(1359-1364).

Kim, K., Kwon, Y. (2008). *Example-based learning for single image super resolution and JPEG artifact removal*. Max Planck Institute for Biological Cybernetics, Technical Report TR-173.

Kohm, K. (2004). Modulation Transfer Function measurement method and results for the ORBVIEW-3 high resolution imaging satellite, *Proceedings of ISPRS annual conference*, Istanbul, Turkey, 2004.

Michelson, A. (1927). *Studies in Optics*. U. of Chicago Press, USA.

Reichenbach, S.E., Park, S.K., Narayanswaury, R. (1991). Characterizing digital image acquisition devices, *Optical Engineering, 30*, pp.(170-177).

Samei, E., Buhr, E., Granfors, P., Vandenbroncke, D., Wang, X. (2005). Comparison of edge analysis techniques for the determination of the MTF of digital radiographic systems, *Phys. Med. Biol. 50*, No.15, pp. (3613–3625).

Shechtman, E., Caspi, Y., Irani, M.(2005). Space-Time Super-Resolution, *IEEE Transactions on Pattern Analysis and Machine Intelligence (PAMI)*, Vol.27, No.4, pp.(531-545).

Shetchman, E., Capsi, Y., Irani, M. (2002). Increasing Space-Time resolution in video, *Proceedings of the 7th European Conference on Computer Vision (ECCV)*, Springer-Vergla, vol.890, Issue 5, pp. (753-768), ISBN: 3540437452.

SIT Technical Note. (1994). *An introduction to scientific imaging charge coupled devices*, Scientific Imaging Technologies. Inc, Beaverton, Oregon, USA.

Spring, K. R., Fellers, T.J., Davidson, M. W. *Introduction to charge coupled devices (CCDs)*, www.microscopyu.com/articles/digitalimaging/ccdintro.html.

Sroubek, F., Flusser, J. (2007). Multiframe blind deconvolution coupled with frame registration and resolution enhancement. *IEEE Transactions on Image Processing*, vol. 16, No. 9, pp. (2322-2332).

Sun, J., Xu, Z., Shum, H. (2008). Image super-resolution using gradient profile prior, *Proceedings of the IEEE conference on Computer Vision and Pattern Recognition (CVPR)*, pp.(1-8), ISBN: 978-1-4244-22425.

Sung Cheol Park, S.C., Park, M. K., Kang. M. M. (2003). Super resolution image reconstruction, a technical overview, *Signal Processing Magazine, IEEE*, Volume 20, Issue 3, May 2003, pp. (21 – 36).

Vandewalle, P., Süsstrunk, S., Vetterli, M. (2006). A Frequency Domain Approach to Registration of Aliased Images with Application to Super-Resolution. *EURASIP Journal on Applied Signal Processing (special issue on Super-resolution)*, Vol. 2006. Article ID 71459, 14 pages.
www.NeutronOptics.com

Williams, D. (2004). Low-Frequency MTF Estimation for Digital Imaging Devices Using Slanted Edge Analysis, *Proc. SPIE-IS&T Electronic Imaging Symposium*, SPIE vol. 5294, pp. (93-101), 2004.

Zomet, A., Rav-Acha, A., Peleg, S. (2001). Robust Super-Resolution, *Proceedings of the international conference on computer vision and pattern recognition (CVPR)*, Hawaii, USA, December 2001, vol.1, pp.(645-650).

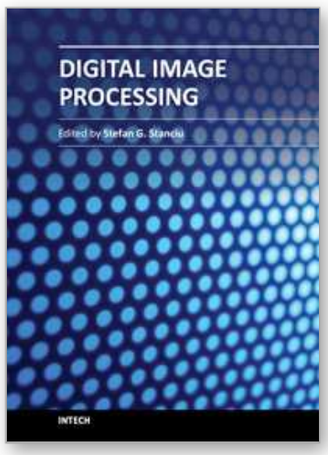

Digital Image Processing

Edited by Dr. Stefan G. Stanciu

ISBN 978-953-307-801-4
Hard cover, 200 pages
Publisher InTech
Published online 11, January, 2012
Published in print edition January, 2012

This book presents several recent advances that are related or fall under the umbrella of 'digital image processing', with the purpose of providing an insight into the possibilities offered by digital image processing algorithms in various fields. The presented mathematical algorithms are accompanied by graphical representations and illustrative examples for an enhanced readability. The chapters are written in a manner that allows even a reader with basic experience and knowledge in the digital image processing field to properly understand the presented algorithms. Concurrently, the structure of the information in this book is such that fellow scientists will be able to use it to push the development of the presented subjects even further.

How to reference

In order to correctly reference this scholarly work, feel free to copy and paste the following:

Faycal Kharfi, Omar Denden and Abdelkader Ali (2012). Temporal and Spatial Resolution Limit Study of Radiation Imaging Systems: Notions and Elements of Super Resolution, Digital Image Processing, Dr. Stefan G. Stanciu (Ed.), ISBN: 978-953-307-801-4, InTech, Available from: http://www.intechopen.com/books/digital-image-processing/temporal-and-spatial-resolution-limit-study-of-radiation-imaging-systems-notions-and-elements-of-sup

INTECH
open science | open minds

InTech Europe
University Campus STeP Ri
Slavka Krautzeka 83/A
51000 Rijeka, Croatia
Phone: +385 (51) 770 447
Fax: +385 (51) 686 166
www.intechopen.com

InTech China
Unit 405, Office Block, Hotel Equatorial Shanghai
No.65, Yan An Road (West), Shanghai, 200040, China
中国上海市延安西路65号上海国际贵都大饭店办公楼405单元
Phone: +86-21-62489820
Fax: +86-21-62489821

IntechOpen